

Mössbauer, magnetic, dielectric and dc conductivity of Al³⁺ ions substituted Mg-Mn-Ni nano ferrite synthesized by citrate precursor method

Satish Verma^{1*}, Jagdish Chand¹, M. Singh²

¹ Department of Physics Govt. P.G. College Solan 173212, India

² Department of Physics Himachal Pradesh University, Summer-Hill, Shimla 171005, India

*Corresponding author. E-mail: satish_apur@yahoo.com

Received: 23 August 2012, Revised: 04 October 2012 and Accepted: 16 October 2012

ABSTRACT

Nanocrystalline Al³⁺ ions doped Mg_{0.2}Mn_{0.5}Ni_{0.3}Al_yFe_{2-y}O₄ compositions, where y=0.0, 0.05 and 0.10 have been synthesized by citrate precursor method. The X-ray diffraction (XRD) revealed that the ferrite has single phase cubic spinel structure. The calculated particle size from XRD data have been verified using transmission electron microscopy (TEM). TEM photographs show that the ferrite powders consist of nanometer-sized particle. It was observed that the particle size decreases as the non-magnetic Al content increases. A decrease in lattice parameter and saturation magnetization with increase in aluminium concentration was attributed to smaller ionic radius and weakening of exchange interaction. Dependence of Mössbauer parameters such as isomer shift, quadrupole splitting and hyperfine magnetic field on Al³⁺ ions concentration have been discussed. Initial permeability μ_i , relative loss factor (RLF), saturation magnetization and remanent magnetization decreases with increasing substitution of Al³⁺ ions. The dielectric constant and dielectric loss decreases with increase in non magnetic Al³⁺ ions. The dielectric constant follows the Maxwell–Wagner interfacial polarization. The electrical conduction in these ferrites is explained on the basis of the hopping mechanism. Copyright © 2013 VBRI press.

Keywords: Mössbauer spectroscopy; initial permeability; dielectric constant; dielectric loss.



Satish Verma is an Associate professor of Physics at Government Post Graduate College, Solan, India. He is Research Scholar registered for Ph.D. under the guidance of Prof. M. Singh Department of Physics, Himachal Pradesh University, Shimla, India. His main research activities include the preparation and study of magnetic behaviour of ferrite materials at nanoscale and Mossbauer spectroscopy.



M. Singh did his Ph.D. in physics from Himachal Pradesh University Shimla in collaboration with Indian Institute of Technology, New Delhi, India in 1995 and M.Phil in 1990 from Himachal Pradesh University Shimla. He is working as Professor in the department of Physics, Himachal Pradesh University Shimla. He is common wealth fellow and his research is focused on semiconductor oxides, diluted magnetic semiconductors, ferrites and multiferroics.



Jagdish Chand did his M.Sc. and M.Phil. from Himachal Pradesh University, Shimla. He is Research Scholar registered for Ph.D. under the guidance of Prof. M. Singh Department of Physics, Himachal Pradesh University, Shimla, India. He is working as an Associate Professor in the department of Physics, Centre of Excellence, Govt. College Sanjauli Shimla-6. His research is focused on electric, dielectric, structural, magnetic and Mossbauer properties of rare earth doped Mg ferrites.

Introduction

Research on nanoparticles has opened an avenue for various potential applications due to their novel properties. Efforts are being continued in bringing out good quality of magnetic cores suitable for ultra-high frequency (microwave) applications. The critical frequency of operation of a ferrite core, in general, is proportional to square of saturation magnetization and DC resistivity and inversely proportional to grain size and initial permeability [1]. The last decade has seen the emergence of particular material properties engineered by exploiting the extraordinary behavior of nanostructures. Nanomaterials are built of components with at least one dimension in the nanometer range. More specifically, dimensions of 1-100 nm are generally considered to fall in this class. At these dimensions, extraordinary physical and chemical properties can be observed, which have formed the basis for a burgeoning nanotechnology industry. It is well known that surface atoms in any material are loosely bound as compared to the interior atoms, hence with increase in surface area the surface free energy increases. Nanomaterials therefore play a very prominent role in physical, chemical and biomedical engineering applications due to their high surface energies [2]. Ferrites are useful magnetic materials because of their versatility, low cost, and high electromagnetic performance over a wide frequency range [3]. The magnetic properties of the nanosized ferrites are entirely different from those of their bulk counterparts, such as the super paramagnetic behavior and associated properties. Nanosized ferrites with uniform particle size and narrow size distribution are desirable for a variety of applications like targeted drug delivery, ferrofluids, medical imaging and other biomedical applications, magnetic data storage, etc. [4].

Ferrites have many applications in heterogeneous catalysis, magnetic materials, refractory materials, medical diagnostics, and in sensors [5]. Spinel oxides based on transition metals such as Ni and Mn are of significant interest, owing to their technological application as negative temperature coefficient (NTC) thermistors for the suppression of in-rush current, temperature measurement and control, and compensation for other circuit elements [6]. Ferrites in nano scale dimension show fascinating and unusual properties compared to their bulk counterparts [7]. In most ferrite materials, the substituents ions play an important role in determining the variation of the physical properties [8].

The investigation of aluminum substituted Mg-Mn-Ni ferrite is not well documented. Electrical conduction in Al^{3+} ions substituted Mg-Mn-Ni ferrite is not yet reported in spite of its potential application at microwave frequencies. In the present work, different concentrations of Al^{3+} ions are used to substitute Fe^{3+} ions at the lattice of Mg-Mn-Ni ferrite to understand the effect of Al^{3+} ions content on structural, electrical and magnetic properties. The Al^{3+} ions substituted ferrites were synthesized by chemical citrate precursor method. By using this technique, particle size, chemical homogeneity and degree of agglomeration can be easily controlled.

Experimental

Materials synthesis and characterization

High purity constituent materials in stoichiometric proportions were used to prepare polycrystalline $\text{Mg}_{0.2}\text{Mn}_{0.5}\text{Ni}_{0.3}\text{Al}_y\text{Fe}_{2-y}\text{O}_4$ sample by citrate precursor method described in ref. [9]. The ferrites series with the composition $\text{Mg}_{0.2}\text{Mn}_{0.5}\text{Ni}_{0.3}\text{Al}_y\text{Fe}_{2-y}\text{O}_4$ ($y=0.0, 0.05$ and 0.10) was prepared using hydrated nitrates of constituent elements. The starting materials for the preparation of Al-series were iron citrate $\text{C}_6\text{H}_5\text{FeO}_7 \cdot 3\text{H}_2\text{O}$ (>98%, BDH laboratory, England), aluminum nitrate $\text{Al}(\text{NO}_3)_3 \cdot 9\text{H}_2\text{O}$ (>98.5%, Merck Germany), citric acid $\text{C}_6\text{H}_8\text{O}_7$ (>99.5%, Merck India), magnesium nitrate $\text{Mg}(\text{NO}_3)_2 \cdot 6\text{H}_2\text{O}$ (>99%, Merck India), manganese nitrate $\text{Mn}(\text{NO}_3)_2 \cdot 4\text{H}_2\text{O}$ (>98.5%, Merck Germany) and nickel nitrate $\text{Ni}(\text{NO}_3)_2 \cdot 6\text{H}_2\text{O}$ (>99%, Merck Germany).

The powder x-ray diffraction (XRD) using the Cu-K α radiation in the 2θ range of $10 - 90^\circ$ was carried out on the samples at room temperature to investigate structural properties. The morphology of samples was studied using Hitachi (H-7500) 120 kV TEM. Initial permeability, relative loss factor, dielectric constant and dielectric loss were measured using an Agilent Technologies 4285A Precision LCR Meter. Magnetization measurements were done using a vibrating sample magnetometer (VSM). ^{57}Fe Mössbauer measurements were carried out in transmission mode with $^{57}\text{Co}/\text{Rh}$ radioactive source in constant acceleration mode using standard PC-based Mössbauer spectrometer equipped with Weissel velocity drive. Velocity calibration was done with natural iron absorber. The spectra were analyzed using least square fitting programme NORMOS (SITE/DIST).

Results and discussion

XRD Study

Average crystallite size D was evaluated by measuring FWHM of most intense peak (311) employing Scherrer's formula [10]:

$$D = K\lambda / B \cos\theta \quad (1)$$

here, λ is wave length of Cu-K α radiation, constant $K=0.9$. Particle size estimated from XRD was 102.25 nm, 44.50 nm and 41.65 nm for $y=0.0, 0.05$ and 0.10 respectively. **Fig. 1** display low resolution TEM image and particle size distribution in $\text{Mg}_{0.2}\text{Mn}_{0.5}\text{Ni}_{0.3}\text{Al}_{0.1}\text{Fe}_{1.9}\text{O}_4$ sample. It can be seen that the particles are quite well dispersed and not much agglomerations are present. An interesting aspect of TEM image is the presence of very small particles coating surface of larger ones. These small particles are nearly evenly sized with an average size ranging from 6-12 nm. Particle size of larger ones, which encloses smaller ones is in the range of about 40-45 nm, which is comparable to particle size determined from Scherrer's formula for $y=0.05$ and 0.10 . The particle size estimated from TEM is slightly less than particle size estimated from XRD using Scherrer's formula. This is because X-ray diffraction gives information of crystalline region only and contribution from amorphous grain surface does not contribute. On other hand TEM gives complete picture of nanoparticles. By analyzing

TEM and XRD one can have almost complete picture of particle size, their distribution and morphology. Lattice constant for $y=0.0$, 0.05 and 0.10 calculated from XRD data was 8.3992 \AA , 8.3947 \AA and 8.3906 \AA respectively. Linear decrease in lattice constant is due to replacement of larger Fe^{3+} ions by smaller Al^{3+} ions. Experimental density and X-ray density decreases with Al^{3+} ions concentration. X-ray density for $y=0.0$, 0.05 and 0.10 were 5.070 g/cm^3 , 5.017 g/cm^3 and 5.014 g/cm^3 respectively. Experimental densities for the same samples were 4.807 g/cm^3 , 4.805 g/cm^3 and 4.801 g/cm^3 .

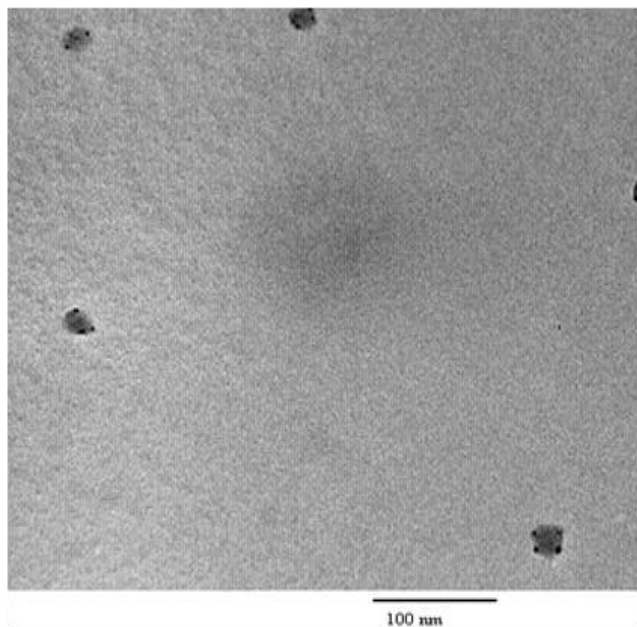


Fig. 1. Low resolution TEM micrograph of sample $\text{Mg}_{0.2}\text{Mn}_{0.5}\text{Ni}_{0.3}\text{Al}_{0.1}\text{Fe}_{1.9}\text{O}_4$ ferrite.

Mössbauer studies

Room temperature Mössbauer spectra of $\text{Mg}_{0.2}\text{Mn}_{0.5}\text{Ni}_{0.3}\text{Al}_y\text{Fe}_{2-y}\text{O}_4$ ($y=0.0, 0.05$ and 0.10) are shown in **Fig. 2**. Dots in figure represent the experimental data and solid lines through the data points are least-squares fitting. The general trend of decreasing the hyperfine fields value is presumably due to the weakening of A–B exchange interaction caused by the substitution of non-magnetic Al^{3+} ions with the Fe^{3+} ions. As indicated, the samples exhibit typical relaxation spectra at room temperature and could be analyzed in terms of the superposition of two sextets and a quadrupole split central line. The Mössbauer phenomenon and the hyperfine interactions have characteristic times and the spectrum observed in any situation depends on whether the properties of the nuclear environment or the position of the nucleus are changing relative to these times. These time-dependent effects can influence both the spectral line shapes and the values of the Mössbauer hyperfine parameters. Time-dependent changes in the nuclear environment are often referred to as relaxation processes. In order to observe the Zeeman splitting between the nuclear energy levels, the magnetic field at the nucleus must remain constant over the period of time T necessary for the nucleus to undergo a Larmor precession of approximately one revolution. The Larmor precession

period T_L for ^{57}Fe is approximately 4×10^{-8} s. A magnetic splitting is observed in Mössbauer spectrum (with six lines in the case of ^{57}Fe) when $T \gg T_L$ and a paramagnetic spectrum (with one or two lines) is observed when $T \ll T_L$. In the intermediate range $T \sim T_L$ (relaxation), complex spectra with broadened lines can be observed. Al^{3+} ions substitution on B-site results in moving some of the Fe^{3+} ions, which has a larger magnetic moment ($5\mu_B$), from B-site to A-site.

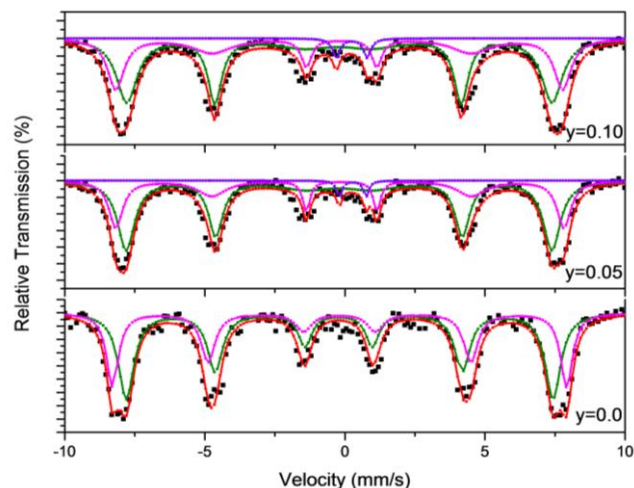


Fig. 2. Mössbauer spectra of $\text{Mg}_{0.2}\text{Mn}_{0.5}\text{Ni}_{0.3}\text{Al}_y\text{Fe}_{2-y}\text{O}_4$ ($y=0.0, 0.05, 0.10$) ferrites.

For $y=0.0$, the occupancies of Fe^{3+} ions at both sites are obtained as nearly equal. On increasing Al content in $\text{Mg}_{0.2}\text{Mn}_{0.5}\text{Ni}_{0.3}\text{Al}_y\text{Fe}_{2-y}\text{O}_4$, total area occupied by Fe^{3+} at A-site was found to increase and that at B-site decreases. This implies that on increasing Al concentration, Al-ions go to the B-site of spinel structure replacing the Fe^{3+} ions from B-site to tetrahedral A-site.

The Mössbauer spectra of samples show a systematic variation with decrease in particle size. As observed from both XRD and TEM studies, particle size decreases with increase in Al^{3+} ions content. Hence variation in the Mössbauer spectra with Al^{3+} ions content can be correlated to particle size. Crystallite sizes are so small that thermally induced energy fluctuations can overcome anisotropy energy and change direction of magnetization of a particle from one easy axis to another, a superparamagnetic relaxation is observed in the Mössbauer spectrum and magnetic sextet collapses into doublets. The presence of doublets alone in the Mössbauer spectra of samples can be attributed to superparamagnetic relaxation due to extremely small size of crystallites [11]. The appearance of paramagnetic doublet superimposed on a two six line pattern indicates presence of short range magnetic ordering induced by fine particle size effects. Al^{3+} ions has no effect on the isomer shifts values, which indicates that the s-electron charge distribution of the Fe^{3+} ions does not change. The isomer shift at A and B sites show that iron is in the Fe^{3+} state.

Quadrupole interaction has values close to zero for both A and B sites. As in the presence of a strong magnetic interaction, the distribution of quadrupole interactions, which arise from chemical disorder, produces an appreciable broadening of the individual Zeeman lines for

both the octahedral and the tetrahedral patterns, but does not produce observable quadrupole line shifts.

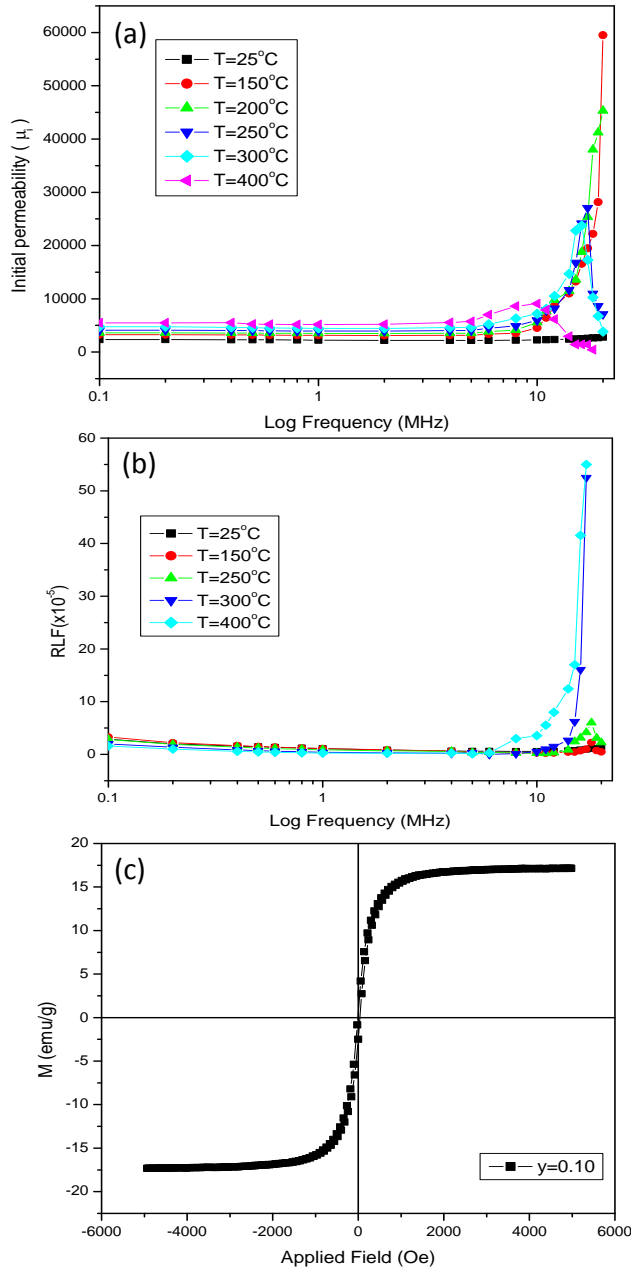


Fig. 3. Variation in (a) initial permeability with frequency at different temperature of $\text{Mg}_{0.2}\text{Mn}_{0.5}\text{Ni}_{0.3}\text{Al}_{0.1}\text{Fe}_{1.9}\text{O}_4$ ferrite., (b) in relative loss factor with frequency at different temperature of $\text{Mg}_{0.2}\text{Mn}_{0.5}\text{Ni}_{0.3}\text{Al}_{0.1}\text{Fe}_{1.9}\text{O}_4$ ferrite and (c) Variation in magnetization with applied field of $\text{Mg}_{0.2}\text{Mn}_{0.5}\text{Ni}_{0.3}\text{Al}_{0.1}\text{Fe}_{1.9}\text{O}_4$ ferrite.

Initial permeability, relative loss factor and saturation magnetization

The variation of ' μ_i ', with frequency at different temperature for $y=0.10$ shown in **Fig. 3(a)** can be explained on basis of Globus model [12]. According to this model, relaxation character is,

$$(\mu_i - 1)^2 f_r = \text{constant} \quad (2)$$

where μ_i is the static initial permeability and f_r is relaxation frequency. Transformation of magnetic spectra from relaxation character to resonance character changes equation (2) to:

$$(\mu_i - 1)^{1/2} f_r = \text{constant} \quad (3)$$

It follows from the above equations that the dispersion frequency is expected to be lower for specimen of higher permeability. This is due to the fact that for materials of lower initial permeability the demagnetizing field, which appear during domain wall movement, results in increasing the restoring force, thereby increasing the relaxation frequency. Citrate precursor method produces ferrites with higher values of initial permeability as such ferrites have less porosity, more uniform grain growth, perfect crystallinity and large number of domain walls. Initial permeability in ferrite is due to domain wall displacement and remains constant with frequency as long as there is no phase lag between applied field and the domain wall displacement. Characteristic property of resonance is present only in those materials which are not homogenous from the point of view of their granular structure and grain size. Resonance character vanishes, because grain size becomes uniform in present work, hence resonance peaks could not be observed. Other reason for not observing resonance peaks is that they may be present at higher frequency, i.e., above 20MHz. Movement of domain walls determines initial permeability and therefore any increase in number of domain walls would result in an increase in initial permeability, μ_i .

Variations of relative loss factor (RLF) i.e. ($\tan \delta / \mu_i$), versus frequency at different temperatures of $\text{Mg}_{0.2}\text{Mn}_{0.5}\text{Ni}_{0.3}\text{Al}_y\text{Fe}_{2-y}\text{O}_4$ for $y=0.10$ is shown in **Fig. 3(b)**. Value of RLF is observed to decrease initially with frequency, reaching a minimum value, and then rise sharply thereafter. Frequency, at which RLF is minimum, called threshold frequency, is observed to vary with temperature. RLF decrease (0.075-10MHz) and then there is increase in RLF up to 20MHz. It decreases with increasing temperature for every composition [13]. RLF has very low value in the range of 10^{-6} - 10^{-5} , which is about three orders of magnitude lower than those reported [14]. In ferrites, two resonance peaks are observed, one due to the domain wall oscillations at lower frequencies and other due to Larmor precession of electron-spins at higher frequencies. From the shape of curves in **Fig. 3(b)**, it is concluded that resonance frequency of domain wall oscillations is slightly higher than 20 MHz. Threshold frequencies, frequency at which relative loss factor is minimum, is observed to shift towards lower frequencies with increase in temperature. Since resonance frequency of domain wall oscillation is inversely proportional to grain size, threshold frequency is expected to shift towards lower frequencies at higher temperatures. Initial permeability and relative loss factor depend on porosity, grain size, magneto-crystalline anisotropy and Fe^{2+} ions concentration. High initial permeability and low RLF are required for high frequency magnetic applications. Factors contributing to low RLF are relatively higher purity of samples prepared by citrate precursor method.

Plots of magnetization (M) vs applied field (H) for $y=0.10$ shown in **Fig. 3(c)**, helps in understanding magnetic

response of material and provides information about magnetic parameters such as saturation magnetization (M_S), coercivity (H_c), remanance magnetization (M_R) and remnant ratio (R). Magnetic hysteresis loops were measured at room temperature. As aluminum content increases, the measured magnetic hysteresis curves become more and more narrow and both the saturation magnetization and remanent magnetization decreases. The observed decrease in saturation magnetization M_S of sample doped with Al^{3+} ions could be attributed to Fe^{3+} ions migration to A-site, which results in reducing magnetic moment of B-site, and consequently a decrease in M_S .

Fe^{3+} and Mn^{2+} ions have random occupancy on A-site and B-site, non-magnetic Mg^{2+} ions have strong preference for B sites and partially occupy A-site, Ni^{2+} and Al^{3+} ions have strong preference to occupy B-site. Magnetic moment per formula unit in Bohr magneton (n_B) was calculated by using following relation:

$$n_B = M \times M_S / 5585 \quad (4)$$

where, M is molecular weight of particular composition and M_S is magnetization at 6 kOe (emu/g). Variation of n_B with changing composition can be explained on basis of Neel's model. According to Neel's two-sublattice model of ferrimagnetism [15], Neel's magnetic moment per formula unit in μ_B , n_B^N is expressed as: $n_B^N(x) = M_B(x) - M_A(x)$, where M_B and M_A are octahedral B and tetrahedral A sublattice magnetic moments in μ_B . With increasing Al^{3+} ions, Fe^{3+} (B) / Fe^{3+} (A) ratio decreases and therefore saturation magnetization and magneton number ' n_B ' decreases. The saturation magnetization (M_S) at room temperature decreases from 56.389 emu/g to 17.516 emu/g and remnant magnetization (M_R) decreases from 4.093 emu/g to 1.942 emu/g due to the doping of Al^{3+} ions in Mg-Mn-Ni ferrite. This decrease in saturation magnetization and remnant magnetization is attributed to the weak magnetic interactions in Mg-Mn-Ni ferrites. Remanent ratio ' R ' = M_R / M_S , is a characteristic parameter of material and is dependent on anisotropy, indicating ease with which magnetization direction is reoriented to nearest easy axis magnetization direction after magnetic field is removed.

Dielectric studies and dc electrical conductivity

The dielectric constant was determined by using the formula:

$$\epsilon' = Cd / \epsilon_0 A \quad (5)$$

where C is the capacitance of the pellet in Farads, d the thickness of the pellet in meters, A the cross-sectional area of the flat surface of the pellet and ϵ_0 is the permittivity constant of free space. The space-charge polarization resulting from electron displacement on application of electric field and the subsequent charge build-up at the insulating grain boundary is a major contributor to the dielectric constant in ferrites. Therefore, more the number of Fe^{2+} ions in the ferrite more would be the space charge polarization expected due to ease of electron transfer between Fe^{3+} and Fe^{2+} ions and consequently higher the dielectric constant.

According to Maxwell-Wagner model, the dielectric

structure of a ferrite material is assumed to be made up of two layers. First layer being a conducting layer consists of large number of grains and the other being grain boundaries is poor conductor. This bi-layer formation is result of high sintering temperature. The polarization results in an electronic exchange between the ferrous and ferric ions, which produce local displacements in the direction of applied external fields. Similarly the $Ni^{3+} \leftrightarrow Ni^{2+} + h$ gives the hole concentration in the octahedral sites which produce the local displacements in the opposite direction of the applied fields. These displacements determine the polarization as well as the dielectric properties. The observed decrease in dielectric constant with increase in frequency is due to the fact that above certain frequency, the electronic exchange between the ferrous and ferric ions does not follow the applied field.

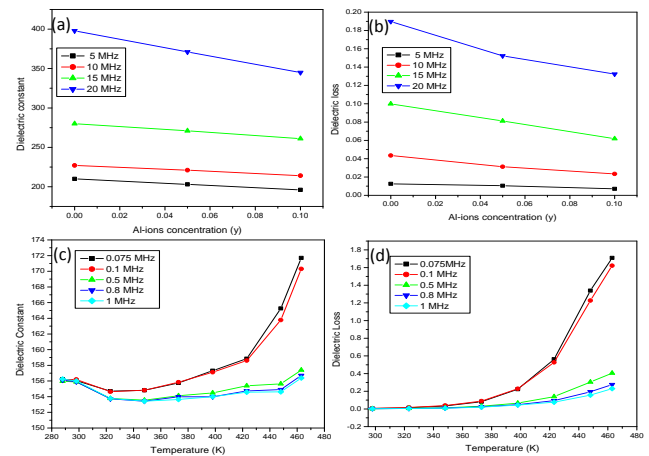


Fig. 4. Variation in (a) dielectric constant with Al-ions concentration at different frequency, (b) dielectric loss with Al-ions concentration at different frequency, (c) dielectric constant with temperature at different frequency of $Mg_{0.2}Mn_{0.5}Ni_{0.3}Al_{0.1}Fe_{1.9}O_4$ ferrite and (d) dielectric loss with temperature at different frequency of $Mg_{0.2}Mn_{0.5}Ni_{0.3}Al_{0.1}Fe_{1.9}O_4$ ferrite.

Fig. 4(a) shows the variation of dielectric constant of $Mg_{0.2}Mn_{0.5}Ni_{0.3}Al_yFe_{2-y}O_4$ ferrites with Al^{3+} ions content (y) measured at room temperature. The dielectric constant decreases with increasing Al^{3+} ions concentration, because of the unavailability of ferrous and ferric ions at the octahedral sites, which are preferentially occupied, by Al^{3+} ions. One main cause of decrease in dielectric constant with Al^{3+} ions is due to the increase in the porosity in Mg-Mn-Ni ferrite. Higher porosity results in lower dielectric constant. The other reason can be explained in view of the hopping conduction mechanism $Fe^{2+} \leftrightarrow Fe^{3+} + e^{-}$. The addition of Al^{3+} ions in place of Fe^{3+} ions limits the degree of conduction and polarization by blocking Verwey's hopping mechanism, which results in the decrease in conductivity and dielectric constant.

Dielectric loss is an important part of the total core loss in ferrites [16]. **Fig. 4(b)** shows the variation of dielectric loss of $Mg_{0.2}Mn_{0.5}Ni_{0.3}Al_yFe_{2-y}O_4$ ferrites with Al^{3+} ions content (y) measured at room temperature. The porosity increases with an increase in Al^{3+} ions content in Mg-Mn-Ni ferrite. Higher porosity results in lower dielectric losses. Hence for low core losses, low dielectric losses are desirable. The dielectric losses in ferrites are reflected in

the conductivity measurements where the materials of high conductivity exhibiting higher losses and vice-versa [10]. The dielectric loss decreases with increasing Al^{3+} ions concentration Fig. 4(b). Thus the present ferrites with relatively lower losses could be useful at higher frequencies.

The variation of dielectric constant with temperature of $\text{Mg}_{0.2}\text{Mn}_{0.5}\text{Ni}_{0.3}\text{Al}_{0.1}\text{Fe}_{1.9}\text{O}_4$ at different frequency is shown in Fig. 4(c). At lower frequencies (0.075 MHz), increase in dielectric constant is very large with an increase in temperature, while at higher frequency (1–5 MHz), the increase in dielectric constant is small. The value of dielectric constant is quite low at room temperature, which is about 10^2 times lower than ferrite samples prepared by the conventional ceramic method [17]. Dielectric constant (ϵ') increases with increase in temperature for all samples; the increase being quite significant at lower frequencies. The value of dielectric constant is high at low frequencies and low at high frequencies. Moreover, increase in value of dielectric constant with increasing temperature is more at low frequencies, than at high frequencies. The dielectric constant of any material, in general, is due to dipolar, electronic, ionic, and interfacial polarizations. At low frequencies dipolar and interfacial polarizations are known to play the most important role. Both these polarizations are strongly temperature-dependent. Whereas the interfacial polarization increases with temperature due to creation of crystal defects, dipolar polarization decreases with increase in temperature. The rapid increase in the dielectric constant with increase in temperature at low frequencies suggests that the effect of temperature is more pronounced on the interfacial than on the dipolar polarization. At high frequencies, electronic and ionic polarizations are the main contributors and their temperature dependence is insignificant. Dielectric constant being inversely proportional to resistivity, decrease in resistivity would result in higher dielectric constant.

The variation of dielectric loss with temperature of $\text{Mg}_{0.2}\text{Mn}_{0.5}\text{Ni}_{0.3}\text{Al}_{0.1}\text{Fe}_{1.9}\text{O}_4$ at different frequency is shown in Fig. 4(d). Just as the dielectric constant curves, the dielectric loss curves also show an increase up to a certain temperature followed by a subsequent decrease, and can be explained on lines similar to those advanced for explaining dielectric constant.

Low losses exhibited by $\text{Mg}_{0.2}\text{Mn}_{0.5}\text{Ni}_{0.3}\text{Al}_y\text{Fe}_{2-y}\text{O}_4$ ($y=0.0, 0.05$ and 0.10) samples up to extended temperature range suggests the applicability of this material at higher frequencies in electrical circuits which experience a high temperature rise.

The observed variation in the conductivity of $\text{Mg}_{0.2}\text{Mn}_{0.5}\text{Ni}_{0.3}\text{Al}_y\text{Fe}_{2-y}\text{O}_4$ as a function of aluminum content at different temperatures is shown in Fig. 5. The conductivity was found to decrease with increasing aluminum content. Fig. 5 also shows that the conductivity of these ferrites increases with increasing temperature exhibiting semiconductor like behavior. In the present study Fe^{3+} ions are partially replaced by Al^{3+} ions. The Al^{3+} ions have strong site preference for B-sites, which leads to the replacement of Fe^{3+} ions at the B-site. Aluminum ions do not participate in the conduction process but limit the degree of $\text{Fe}^{2+} \leftrightarrow \text{Fe}^{3+}$ conduction by blocking up the

$\text{Fe}^{2+} \leftrightarrow \text{Fe}^{3+}$ transformation. This phenomenon hinders the Verwey-de Boer mechanism between statistically distributed Fe^{2+} and Fe^{3+} ions at the equivalent crystallographic lattice sites, resulting in a decrease in the conductivity. A–A hopping does not exist as there are only Fe^{3+} ions on this sublattice and any Fe^{2+} ions formed during processing preferentially occupy the B sites. B–B hopping is more dominant than A–B hopping. This explains the observed decrease in conductivity with increasing aluminum content in the ferrites.

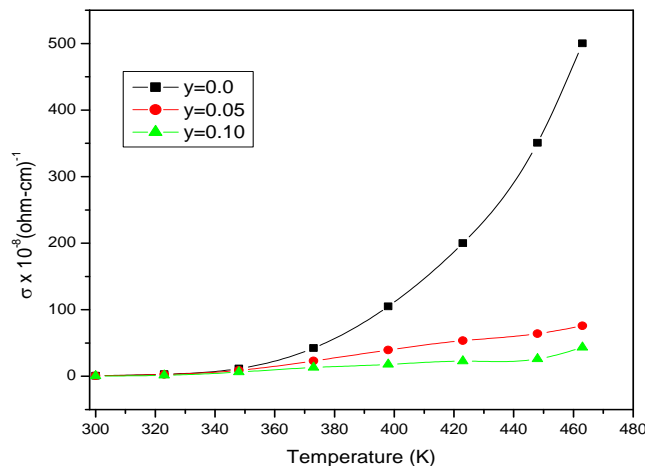


Fig. 5. Variation of Dc electrical conductivity with temperature of $\text{Mg}_{0.2}\text{Mn}_{0.5}\text{Ni}_{0.3}\text{Al}_y\text{Fe}_{2-y}\text{O}_4$ ferrites.

Conclusion

$\text{Mg}_{0.2}\text{Mn}_{0.5}\text{Ni}_{0.3}\text{Al}_y\text{Fe}_{2-y}\text{O}_4$ ($y=0.0, 0.05$ and 0.10) ferrites were successfully synthesized by citrate precursor technique. The nanosized ferrites, formed are super paramagnetic. Room temperature Mössbauer spectra of as obtained samples exhibit broad doublet suggesting super paramagnetic nature. Mössbauer spectral studies show collapse of magnetic ordering due to smaller particle size. Incorporation of Al^{3+} ions in Mg-Mn-Ni ferrite results in decrease in lattice parameter, particle size, initial permeability, relative loss factor, saturation magnetization and remanent magnetization. Relative loss factor at room temperature is of the order of 10^{-6} – 10^{-5} . Low values of RLF and high resistivity exhibited by these ferrites suggest its utility in high frequency applications. With Al^{3+} content conductivity, dielectric constant and dielectric loss of the samples decreases.

Reference

- Mahesh Kumar, A.; Chaitanya Varma, M.; Choudary, G.S.V.R.K.; Prameela, P.; Rao, K.H. *J. Magn. Magn. Mater.* **2012**, 324, 68-71. DOI: [10.1016/j.jmmm.2011.07.045](https://doi.org/10.1016/j.jmmm.2011.07.045)
- Tiwari, Ashutosh.; Mishra, Ajay K.; Kobayashi, Hisatoshi.; Turner, Anthony P.F. *Intelligent Nanomaterials* Wiley-Scrivener Publishing LLC, USA, 2012, ISBN 978-04-709387-99.
- Dixit, Gagan.; Singh, J.P.; Srivastava, R.C.; Agrawal, H.M.; Chaudhary, R.J. *Adv. Mat. Lett.* **2012**, 3(1), 21-28. DOI: [10.5185/amlett.2011.6280](https://doi.org/10.5185/amlett.2011.6280)
- Kaur, Balwinder.; Arora, Manju.; Shankar, Ajay.; Srivastava, Avanish Kumar.; Pant, Rajendra Prasad. *Adv. Mat. Lett.* **2012**, 3(5), 399-405. DOI: [10.5185/amlett.2012.7288](https://doi.org/10.5185/amlett.2012.7288)
- Jagdish et al. *J. Alloys Compd.* **2011**, 509, 9638. DOI: [10.1016/j.jallcom.2011.07.055](https://doi.org/10.1016/j.jallcom.2011.07.055)

6. Wang, Jiangying.; Zhang, Jingji. *J. Mater.Sci. Engg.* **2011**, B 176, 616-619.
DOI: [10.1016/j.mseb.2011.01.020](https://doi.org/10.1016/j.mseb.2011.01.020)
7. Pradeepa, A.; Priyadharsini, P.; Chandrasekaran, G. *J. Alloys Compd.* **2011**, 509, 3917-3923.
DOI: [10.1016/j.jallcom.2010.12.168](https://doi.org/10.1016/j.jallcom.2010.12.168)
8. Ahmed, M.A.; Mansour, S.F.; Afifi, M. *J. Magn. Magn Mater.* **2012**, 324, 4-10.
DOI: [10.1016/j.jmmm.2011.07.010](https://doi.org/10.1016/j.jmmm.2011.07.010)
9. Verma, Satish.; Chand, Jagdish.; Singh, M. *J. Magn. Magn Mater.* **2012**, 324, 3252-3260.
DOI: [10.1016/j.jmmm.2012.04.053](https://doi.org/10.1016/j.jmmm.2012.04.053)
10. Chand, Jagdish.; Singh, M. *J. Alloys Compd.* **2009**, 486, 376.
DOI: [10.1016/j.jallcom.2009.06.150](https://doi.org/10.1016/j.jallcom.2009.06.150)
11. Mandal, K.; Mandal, S.P.; Agudo, P.; Pal, M. *Appl. Surf. Sci.* **2001**, 182, 386.
DOI: [10.1016/S0169-4332\(01\)00455-X](https://doi.org/10.1016/S0169-4332(01)00455-X)
12. Globus, A.; Duplex, P.; Guyot, M. *IEEE Trans.Magn.Magn.* **1971**, 7, 617.
DOI: [10.1109/TMAG.1971.1067200](https://doi.org/10.1109/TMAG.1971.1067200)
13. Kramar, G. P.; Panova, Y. I. *Phys. Stat. Sol.* **1983**, 77, 483.
DOI: [10.1002/pssa.2210770210](https://doi.org/10.1002/pssa.2210770210)
14. Razzite, A.C.; Jacob, S. E.; Fano, W. G. *J. Appl. Phys.* **2000**, 87, 6232.
DOI: [10.1063/1.372664](https://doi.org/10.1063/1.372664)
15. Chauhan, B.S.; Kumar, R.; Jadhav, K.M.; Singh, M. *J. Magn. Magn Mater.* **2004**, 283, 71.
DOI: [10.1016/j.jmmm.2004.04.133](https://doi.org/10.1016/j.jmmm.2004.04.133)
16. Zhu, J.; Tseng, K.J.; Foo, C.F. *IEEE Trans. Magn.* **2000**, 36 (5), 3408.
DOI: [10.1109/20.908842](https://doi.org/10.1109/20.908842)
17. Koops, C.G. *Phys. Rev.* **1951**, 83, 121.
DOI: [10.1103/PhysRev.83.121](https://doi.org/10.1103/PhysRev.83.121)

Advanced Materials Letters

Publish your article in this journal

[ADVANCED MATERIALS Letters](#) is an international journal published quarterly. The journal is intended to provide top-quality peer-reviewed research papers in the fascinating field of materials science particularly in the area of structure, synthesis and processing, characterization, advanced-state properties, and applications of materials. All articles are indexed on various databases including [DOAJ](#) and are available for download for free. The manuscript management system is completely electronic and has fast and fair peer-review process. The journal includes review articles, research articles, notes, letter to editor and short communications.

